COMMUNICATIONS ON
PURE AND APPLIED ANALYSIS
Volume **11**, Number **1**, January **2012**

doi:10.3934/cpaa.2012.11.261

pp. **261–273**

OSTWALD RIPENING IN DRYLAND VEGETATION

Assaf Y. Kletter

Department of Physics
Ben-Gurion University, Beer-Sheva, 84105, Israel

Jost von Hardenberg

Institute of Atmospheric Sciences and Climate - CNR
C.so Fiume 4, 10133, Torino, Italy

Ehud Meron

Institute for Dryland Environmental Research
Ben-Gurion University, Sede Boqer Campus, 84990, Israel
and Department of Physics
Ben-Gurion University, Beer-Sheva, 84105, Israel

Abstract. Dryland landscapes self-organize to form various patterns of vegetation patchiness. Two major classes of patterns can be distinguished: regular patterns with characteristic length scales and scale-free patterns. The latter form under conditions of global competition over the water resource. In this paper we show that the asymptotic dynamics of scale-free vegetation patterns involve patch coarsening similar to Ostwald ripening in two-phase mixtures. We demonstrate it numerically, using a spatially explicit model for water-limited vegetation, and further study it by drawing an analogy to an activator-inhibitor system that shares many properties with the vegetation system. The ecological implications of patch coarsening may not be highly significant due to the long time scales involved. The reported results, however, raise an interesting pattern formation question associated with the incompatibility of mechanisms that stabilize vegetation spots and the condition of global competition.

1. **Introduction.** Patterns in nature often show regular structures with characteristic length scales. Cloud streets and vegetation bands in drylands are two striking examples. The emergence of a characteristic length is attributed to self-organization mechanisms, such as shear and thermal instabilities in the case of cloud streets [1] and positive biomass-water feedbacks in the case of banded vegetation [2]. Numerous experimental and theoretical studies of fluid, chemical and optical systems, have established the relation between periodic spatiotemporal patterns and symmetry breaking instabilities, thereby confirming the interpretation of periodic patterns in nature as self-organization phenomena.

Natural patterns, however, do not necessarily possess characteristic lengths. In fact, irregular scale-free patterns are more common in nature than regular periodic patterns. Unlike periodic patterns, the association of scale-free patterns with self-organization mechanisms is not obvious, for nonuniform environmental conditions, which always exist in natural settings, may override such mechanisms and account

2000 *Mathematics Subject Classification.* Primary: 58F15, 58F17; Secondary: 53C35.

Key words and phrases. Pattern formation, vegetation patterns, activator-inhibitor systems, scale-free patterns, phase coarsening.

for the lack of scale. An interesting context for studying the possible emergence of scale-free patterns as a self-organization phenomenon is vegetation patchiness in water limited systems. Recent field studies reported the observations of scale-free vegetation patterns with power-law like patch-size distributions [3, 4]. Following these reports, theoretical efforts to reconcile the observations of periodic and scale-free patterns, have begun [5, 6]. These studies, based on simple [5] and more elaborate [6, 7, 8] models, have identified fast water transport, relative to water exploitation, as a factor that can induce scale-free patterns, and described physical and ecological conditions under which such time-scale separation can be realized [6].

While the predictions of these model studies await experimental tests, there are several theoretical issues that need further clarification. One such issue is whether scale-free patterns, in the context of dryland vegetation and other contexts as well, are long transients or asymptotic patterns. In this paper we address this question by drawing an analogy between the vegetation model studied in Ref. [6] and a simpler activator-inhibitor model. We begin in section 2 with a review of model studies of periodic and scale-free vegetation patterns and present new model simulations suggesting that scale-free patterns are transients undergoing a phase coarsening process. In section 3 we reproduce the phenomenology of the vegetation model with the activator-inhibitor model, and use the latter to study the phase coarsening process. We conclude in section 4 with a brief summary and discussion of the results.

2. **Vegetation patch dynamics.**

2.1. **The model.**

As evidenced by several studies, vegetation patterning in drylands can result from feedback processes between water and biomass acting at different spatial scales. In particular mechanisms of local facilitation, coupled with long-range mechanisms of competition for the scarce water resource, have been found to play crucial roles. Increased infiltration under vegetation patches and shading represent important local facilitation processes, while overland water flow and competition through the root system are examples of important long-range feedbacks. A wide class of deterministic models, commonly based on PDEs, has been developed to encompass these mechanisms [9]. They range from simple one-compartment models representing only biomass[10, 11], to models separating the distribution of water in the soil from surface flows [12, 7]. One important result of these studies is their robustness and consistency: all models are capable of reproducing the same phenomenology of periodic biomass patterns as soon as realistic ranges are chosen for the parameters. They differ mainly in the detail with which they represent different feedback mechanisms, enabling some of them to capture in richer detail the phenomenology of vegetation patterns, their resilience to environmental changes, or the creation of ecological niches. In particular the model used in [6], falls into this class: it includes all main feedbacks considered in other models with the addition of non-local feedbacks associated with water uptake by spatially extended root systems, and the associated long-range competition. Thanks to its versatility the model could be applied to various distinct contexts of dryland vegetation including the effects of environmental conditions on pattern formation and resilience, pattern transitions, ecosystem engineering, species coexistence and the impact of rainfall intermittency [7, 8, 13, 14, 15, 16, 17, 18]. The model has also been shown to reproduce both periodic and scale-free pattern states [6].

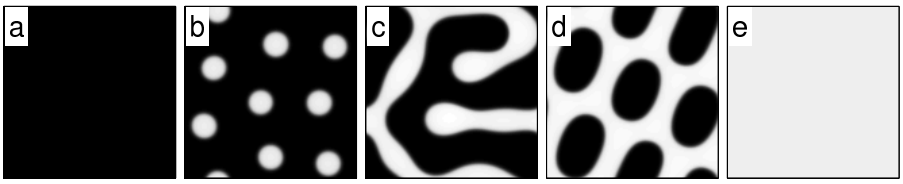

FIGURE 1. The five basic pattern states predicted by the vegetation model at different precipitation rates (light color denotes high biomass). Bare soil (a), spots (b), stripes (c), holes (d), uniform vegetation (e). The parameter values correspond to shrubs in arid areas, see [8], with $\rho = 10$. The precipitation rates correspond to 75 mm/yr (a), 225 mm/yr (b), 675 mm/yr (c), 990 mm/yr (d), 1800 mm/yr (e). The domain size is $L = 4 \times 4$ m^2 and the integration time is 833 yr.

We describe the dynamics of dryland vegetation using three non-dimensional variables: biomass per unit area, $b(\mathbf{x}, t)$, soil water density, $w(\mathbf{x}, t)$, and the height of a thin layer of water above ground surface, $h(\mathbf{x}, t)$, where $\mathbf{x} = (x, y)$ is space and t is time. The precipitation rate p represents the main control parameter in this study. We refer the reader to Ref. [8, 18] for a detailed description of the model and for a description of its non-dimensional form. On a plane topography, in non-dimensional units, the model equations can be written as:

$$\begin{aligned} b_t &= \mathcal{G}_b b(1-b) - b + \delta_b \nabla^2 b \\ w_t &= \mathcal{I}h - \mathcal{E}w - \mathcal{G}_w w + \delta_w \nabla^2 w \\ h_t &= p - \mathcal{I}h + \delta_h \nabla^2 (h^2)\,, \end{aligned} \tag{1}$$

where $\mathcal{E}(b)$, $\mathcal{I}(b)$, $\mathcal{G}_b(b, w)$ and $\mathcal{G}_w(b)$ are functionals of the variables representing the feedback processes at work in the problem. In particular $\mathcal{E}(b) = \nu/(1+\rho b)$ represents locally reduced evaporation due to vegetation (shading feedback), $\mathcal{I}(b) = \alpha(b+qf)/(b+q)$ represents increased infiltration under vegetation patches (infiltration feedback) and the two integral terms $\mathcal{G}_b(b, w) = \nu \int g(\mathbf{x}, \mathbf{x}', t) w(\mathbf{x}', t) d\mathbf{x}'$ and $\mathcal{G}_w(b) = \gamma \int g(\mathbf{x}', \mathbf{x}, t) b(\mathbf{x}', t) d\mathbf{x}'$, with $g(\mathbf{x}, \mathbf{x}', t) = \frac{1}{2\pi} \exp\left[-\frac{|\mathbf{x}-\mathbf{x}'|^2}{2[1+\eta b(\mathbf{x},t)]^2}\right]$, represent increased vegetation growth and depletion of soil humidity due to root uptake (root feedback). All other quantities are constant parameters. The correspondence between non-dimensional and dimensional units and parameters is described in detail in [8].

2.2. **Regular patterns.** In a wide range of parameter values, appropriate for describing vegetation in water-limited environments, uniform-vegetation solutions of the model (1) are found to be linearly unstable to finite wavelength spatial perturbations. The dynamics in this range lead to the development of five different basic pattern states along gradients of increasing precipitation as shown in Fig. 1: bare soil, spots (approaching an hexagonal pattern), vegetation bands or labyrinths, holes in uniform coverage (approaching an hexagonal pattern), and uniform vegetation coverage. Moreover, any consecutive pair of basic states along the precipitation axis has a bistability range in which spatially mixed patterns are generally realized as shown in Fig. 2. These bistability ranges also imply hysteretic state transitions

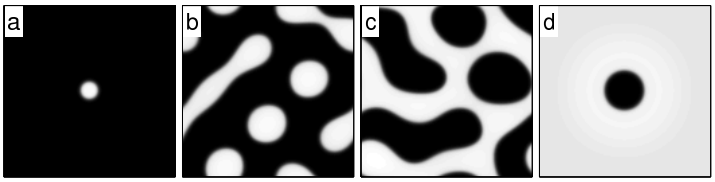

FIGURE 2. Bistability ranges of basic states give rise to spatially mixed patterns: bare soil and spots (a), spots and stripes (b), stripes and holes (c), holes and uniform vegetation (d). The parameter values are as in Fig. 1 with precipitation rates corresponding to 90 mm/yr (a), 570 mm/yr (b), 900 mm/yr (c), and 1725 mm/yr (d). The domain size is $L = 4 \times 4$ m^2 and the integration time is 830 yr.

[16, 19]. The emergence of periodic patterns is mainly a result of the ability of vegetation patches to draw water from their neighborhoods either by inducing overland flow, or by soil-water uptake through spatially extended root systems.

2.3. **Scale-free patterns and patch coarsening.** As discussed in detail in [6], the model (1) also reproduces scale-free patterns, where no characteristic length scale can be identified, under conditions where the competition for the resource acts over very long distances. Examples of such situations are areas where surface water flows over long distances before infiltrating into the soil, or where long-range soil-water exchanges occur before significant uptake takes place. Common to all these situations is the presence of a mechanism for fast horizontal water transport relative to processes that absorb or exploit the water resource. Under this condition competition for water acts globally and imposes a global constraint on the maximal sustainable biomass. If other mechanisms that limit patch growth, such as strong root feedback, are inhibited, patch growth can be unbounded, leading to the emergence of scale-free patterns [6] as Fig. 3(a) shows.

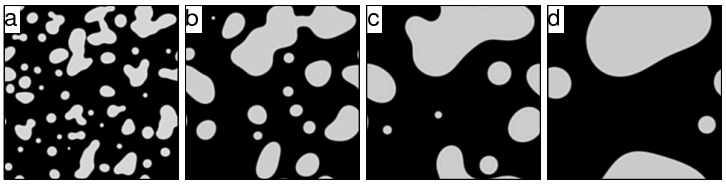

FIGURE 3. Development of scale free patterns (a) followed by patch coarsening (b,c,d) in the vegetation model starting from an initial random perturbation of the uniform bare-soil state. The snapshots were taken after 87 (a), 500 (b), 1500 (c) and 4,580 years (d). The parameter values are as in Fig. 1, except for $\eta = 0$ and $\delta_h = \infty$, with a precipitation rate corresponding to 120 mm/yr. The domain size is $L = 32 \times 32$ m^2.

An important issue which still remained to be clarified in [6] is whether scale-free vegetation patterns represent stationary asymptotic states. To study this question, we performed a few very long simulations of the vegetation model, under conditions

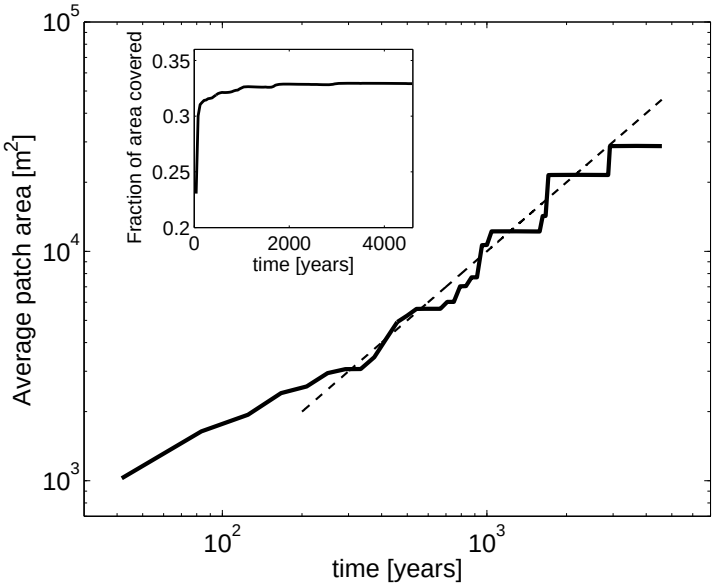

FIGURE 4. The average patch area as a function of time for the data of figure 3. The dashed reference line indicates a linear growth with time. The inset shows the fraction of area covered by vegetation as a function of time. To produce this graph we identified the surface covered by connected areas with vegetation larger than 0.05 Kg/m^2.

of fast surface-water flow and reduced root feedback, and we display one example in Figs. 3 and 4. It is evident from these figures that while the overall fraction of area covered by vegetation (see inset in Fig. 4) and the total biomass asymptote quickly to equilibrium constant values, determined by the actual precipitation rate, the pattern itself continues evolving, with growth and merger of patches, approaching eventually an asymptotic state containing a single circular patch. During this patch-coarsening process the average patch size grows linearly in time as Fig. 4 shows.

3. **Activator-inhibitor dynamics.**

3.1. **The FitzHugh-Nagumo model.** The water-limited vegetation system discussed in Sec. 2 can be regarded as an activator-inhibitor system, where the activator is the above-ground biomass and the inhibitor is lack of soil-water. Biomass growth induces (activates) lack of water by water uptake, while lack of water inhibits biomass growth. In this respect we can draw an analogy between the vegetation model (1) and a modified version of the FitzHugh-Nagumo (FHN) model:

$$u_t = g(u) - v + \nabla^2 u \tag{2}$$

$$v_t = \epsilon(u - a_1 v - a_0) + \delta\nabla^2 v\,, \tag{3}$$

where

$$g(u) = u + bu^3 - cu^5\,. \tag{4}$$

Here, u is the activator, v is the inhibitor and a_0, a_1, b, c, ϵ, δ are constant parameters. Apart of a_0 and b, which can be negative, and c which can be zero, all other parameters are positive. In addition, we assume that $\delta > 1$. The stationary uniform solutions of (3) are given by the intersection points of the nonlinear nullcline $g(u) - v = 0$ and the linear nullcline $u - a_1 v - a_0 = 0$. We focus here on the case of a single intersection point (u_0, v_0) at the middle branch of the nonlinear nullcline. In the symmetric case, where $a_0 = 0$, this intersection point describes a zero equilibrium state $(u_0, v_0) = (0, 0)$. Depending on the values of ϵ and δ the equilibrium state (u_0, v_0) can lose stability to uniform oscillations in a Hopf bifurcation, or to stationary periodic patterns in a Turing bifurcation. A linear stability analysis gives the following thresholds for the Hopf (ϵ_H) and Turing (ϵ_T) bifurcations:

$$\epsilon_H = \frac{g'(u_0)}{a_1}\,, \quad \epsilon_T = \frac{\delta}{2 - a_1 g'(u_0) + 2\sqrt{1 - a_1 g'(u_0)}}\,. \tag{5}$$

The Turing instability results from long-range competition induced by fast inhibitor diffusion to the neighborhoods of growing-activator areas.

3.2. **Regular patterns.** The vegetation model has five basic vegetation states along the rainfall gradient and many more spatially mixed states in the bistability ranges of adjacent basic states. The existence and stability of localized spot solutions in the bistability range of bare soil and spots and of localized hole solutions in the bistability range of uniform vegetation and holes, are likely to be related to homoclinic snaking [20, 21].

To obtain an analogous behavior in the FHN model we look for conditions that give rise to a subcritical Turing instability of the equilibrium state (u_0, v_0). Such conditions imply a bistability range of a uniform and a patterned state in which localized solutions are expected to be found. A weak nonlinear analysis of the symmetric ($a_0 = 0$) FHN model, in one space dimension and in the vicinity of the Turing instability, gives the approximate solution

$$u \approx A e^{ik_T x} + c.c.\,, \qquad v \approx (1 - k_T^2) A e^{ik_T x} + c.c.\,, \tag{6}$$

where the Turing wavenumber k_T is given by

$$k_T^2 = \frac{\sqrt{1 - a_1 g'(u_0)} - [1 - a_1 g'(u_0)]}{a_1}\,, \tag{7}$$

and the amplitude A satisfies (up to 3rd order in the amplitude)

$$A_t = \frac{\lambda \delta k_T^2}{\delta - 1} A + 3\frac{\delta b}{\delta - 1}|A|^2 A + 4\frac{\delta\sqrt{1 - a_1}}{\delta - 1} A_{xx}\,. \tag{8}$$

Here $\lambda = (\epsilon_T - \epsilon)/\epsilon_T$ is the deviation from the Turing instability. The condition for a subcritical Turing instability is that the sign of the cubic term is positive (in which case the analysis should be continued to 5th order in order to get stable Turing-pattern solutions). Since $\delta > 1$, a subcritical bifurcation in the symmetric FHN model is obtained for $b > 0$. Choosing $b > 0$ and large enough, we can guarantee a subcritical bifurcation for the non-symmetric ($a_0 \neq 0$) FHN model too.

A glance at Eq. (3) reveals that the parameter a_0 plays a similar role to the precipitation parameter p in the vegetation model. They both control the input sources for the inhibitor; an increase of a_0 leads to a decrease of the inhibitor v, very much like an increase of p which reduces the lack of soil water. Indeed, solving numerically the FHN model with $b = 1$ and $c = 1$ for increasing values of a_0, we

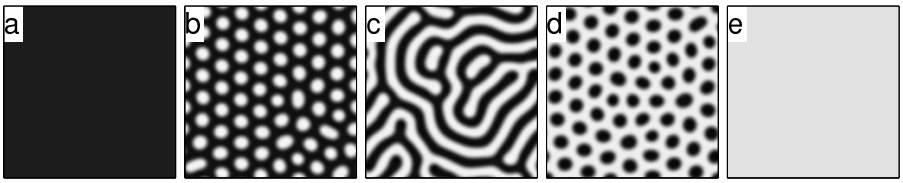

FIGURE 5. The five basic states of dryland vegetation (Fig. 1) reproduced with the FHN model (Eqs. 2 and 3) along the a_0 axis: uniform down state (panel a), spots (b), stripes (c), holes (d) and uniform up state (e). Parameters: $a_1 = 0.8$, $\epsilon = 3.2$, $\delta = 7.5$, $b = c = 1$ and a_0 changes from -0.08 in panel (a) through $-0.05, 0, 0.05$ (panels b,c and d, respectively) to 0.08 in panel (e). The domain size is $L = 100 \times 100$ and the integration time is 400.

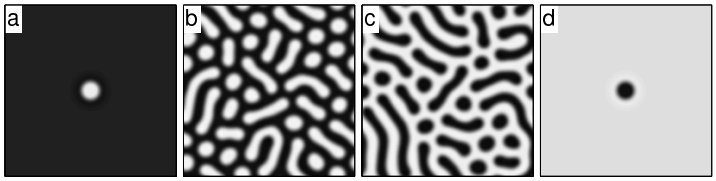

FIGURE 6. Spatially mixed states obtained in bistability ranges of any consecutive pair of basic states in the FHN model (Eqs. 2 and 3): isolated spot (panel a), spots and stripes (b), stripes and holes (c) and isolated hole (d). Parameters are as in Fig 5, except for $a_0 = -0.06$ in panel (a), $a_0 = -0.02$ (b) $a_0 = 0.02$ (c) and $a_0 = 0.06$ in panel (d). The domain size is $L = 100 \times 100$ and the integration time is 400.

find the same basic states of the vegetation model, as Fig. 5 shows. We also find bistability ranges that give rise to stable spatial mixtures of any pair of consecutive basic states, as Fig. 6 shows, including localized structures analogous to a single vegetation patch and to a single vegetation hole.

3.3. **Scale-free patterns.** The condition of fast water transport relative to water exploitation in the vegetation model amounts to fast inhibitor diffusion relative to inhibitor production in the FHN model, or to $\delta/\epsilon \gg 1$. To avoid Hopf oscillations we choose $\epsilon > \epsilon_H \sim O(1)$, and therefore require $\delta \gg 1$. In this range we can approximate $\nabla^2 v = 0$. Assuming periodic or Neumann boundary conditions, we deduce that $v = v(t)$ is uniform in space, and averaging Eq. (3) over space we obtain

$$v_t = \epsilon(\langle u \rangle - a_0 - a_1 v)\,, \tag{9}$$

where $\langle u \rangle$ is the spatial average of u. Note that $\delta \nabla^2 v$ is not necessarily small and the absence of this term in Eq. (9) is due to the spatial averaging. The vegetation counterpart to Eq. (9) in the limit of fast surface-water flow relative to infiltration is $h_t = p - \langle \mathcal{I} \rangle h$, obtained from the equation for h in (1) in the limit $\delta_h \to \infty$.

Numerical simulations of Eqs. (2) and (9), starting with random initial conditions about the equilibrium state (u_0, v_0) reveal a remarkably different behavior than that

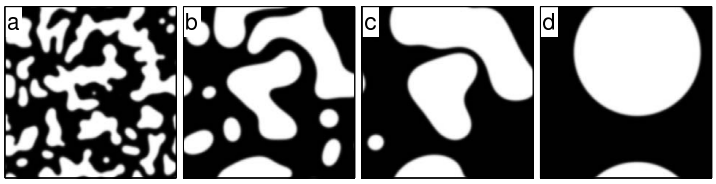

FIGURE 7. Development of scale free patterns (a) followed by phase coarsening (b,c) and the convergence to a single spot (d) in Eqs. (2) and (9). Parameters: $b = -1$, $c = 0$, $a_0 = -0.15$, $a_1 = 0.5$, $\epsilon = 3.0$. Snapshots were taken at $t = 15$ (a), $t = 100$ (b), $t = 250$ (c) and $t = 9250$ (d). The domain size is $L = 200 \times 200$.

described in Sec. 3.2. Instead of regular Turing patterns with characteristic length scales, irregular scale-free patterns develop, as Fig. 7(a) shows. However, on a longer time scale a phase coarsening process begins (Fig. 7(b-d) whereby small spots shrink and disappear while big spots grow and merge together. During this process the spot boundaries smooth out and approach circular forms. This behavior is similar to that found in the vegetation model in the limit of fast water transport and is reminiscent of Ostwald ripening in two-phase mixtures [22, 23, 24, 25, 26].

To gain a better understanding of the emergence of scale-free patterns and the phase-coarsening processes that follows, we analyze Eqs. (2) and (9), assuming $|v| \ll 1$. The consistency of this assumption will be tested later on. Equation (2) is the time-dependent Ginzburg-Landau equation, subjected to a small fluctuating field v that satisfies (9). We will first analyze this equation in one space dimension. We will see that it has front solutions that separate domains of high and low u values (hereafter "up-state" and "down-state" domains), which describe the boundaries of "one-dimensional spots". Let Γ be the time-dependent position of a front solution. For $v = 0$ the front is stationary and Γ is constant, while for $|v| \ll 1$ the front is slowly propagating. We quantify the smallness of v by introducing a small auxiliary parameter $\mu \ll 1$, and describe the slow front propagation by $\Gamma = \Gamma(\tau)$, where $\tau = \mu t$ is a slow time coordinate. We now introduce a moving coordinate frame $z = x - \Gamma(\tau)$, and express Eq. (2) in terms of $u(z, \tau)$ and $v(\tau)$ as

$$\mu u_\tau - \mu \frac{d\Gamma}{d\tau} u_z = g(u) - v + u_{zz} \,. \tag{10}$$

For simplicity we use the same notations for u and v even though they are now expressed as functions of the new coordinates z and τ. Expanding u and v as

$$u(z, \tau) = u_0(z) + \mu u_1(z, \tau) + \dots \,, \qquad v(\tau) = \mu v_1(\tau) + \dots \,, \tag{11}$$

we obtain at order unity,

$$u_{0zz} + g(u_0) = 0 \,. \tag{12}$$

Equation (12) has front solutions that are biasymptotic to a symmetric pair of uniform states, u_+ and $u_- = -u_+$, the up and down states, that satisfy $g(u_\pm) = 0$. For the specific choice of $b = -1$ and $c = 0$ in (4), $u_\pm = \pm 1$ and $u_0 = \pm \tanh(z/\sqrt{2})$. These front solutions are the leading order approximations for the boundaries of one-dimensional spots.

At order μ we obtain

$$\mathcal{L} u_1 = v_1 - \frac{d\Gamma}{d\tau} u_{0z} \,, \tag{13}$$

where

$$\mathcal{L} \equiv \frac{\partial^2}{\partial z^2} + g\prime(u_0)\,, \tag{14}$$

and the prime denotes derivative with respect to the argument. The linear operator $\mathcal{L}$ is singular since

$$\mathcal{L}u_{0z} = 0\,. \tag{15}$$

Solvability of (13) then gives

$$\frac{d\Gamma}{d\tau} = \alpha v_1\,, \qquad \alpha = \frac{\int_{-\infty}^{\infty} u_{0z}dz}{\int_{-\infty}^{\infty}(u_{0z})^2 dz}\,, \tag{16}$$

or in terms of the original time

$$\dot{\Gamma} = \alpha v\,. \tag{17}$$

For a front that is biasymptotic to $u_\pm$ as $z \to \mp\infty$, α is negative. For the specific choice, $b = -1$ and $c = 0$ (and for $|v| \ll 1$), $\alpha = -3/\sqrt{2}$.

These results for front solutions have interesting implications for one-dimensional solutions of Eqs. (2) and (3) that describe stationary patterns in the limit $\delta \to \infty$. Since the boundaries of the spots that comprise a stationary pattern must be stationary too, we have $\dot{\Gamma} = 0$. Equations (17) and (9) then give

$$v = 0\,, \qquad \langle u\rangle = a_0\,. \tag{18}$$

Thus, stationary pattern solutions should satisfy the global constraint $\langle u\rangle = a_0$. To evaluate the stability of such solutions we first argue that $\langle u\rangle$ is a decreasing function of v. The dependence of $\langle u\rangle$ on v comes through the values of the up and down states, $u_\pm(v)$, and through the widths of the up and down-state domains. The up and down states are decreasing functions of v. This is implied by the form (4) of $g(u)$. For the choice $b = -1$ and $c = 0$, for example, $u_\pm = \pm 1 - v/2$ (for $|v| \ll 1$). The widths of the up-state domains are also decreasing functions of v, because positive v implies $\dot{\Gamma} < 0$ for a front biasymptotic to $u_\pm$ as $z \to \mp\infty$, and $\dot{\Gamma} > 0$ for a front biasymptotic to $u_\pm$ as $z \to \pm\infty$. Similarly, the widths of the down-state domains are increasing functions of v. Since decreasing the values of the up and down states, decreasing the widths of the up-state domains, and increasing the widths of the down-state domains all lower the value of $\langle u\rangle$, we conclude that $\langle u\rangle \equiv h(v)$ must be a decreasing function. Writing Eq. (9) as $v_t = f(v)$ where $f(v) = \epsilon(h - a_1 v - a_0)$ we find that $f'(0) < 0$ which implies the linear stability of the stationary solutions to perturbations along the v axis, and justifies the assumption $|v| \ll 1$.

The analysis described above does not take into account the interactions between nearby domains and therefore does not give us information about the asymptotic solutions that satisfy the global constraint (18). These interactions, however, are exponentially weak [27, 28], and apart of transients during which sufficiently nearby domains attract and merge, the dynamics freeze on an apparently stationary pattern, as Fig. 8 demonstrates. Depending on initial conditions, scale-free patterns can develop.

3.4. **Phase coarsening.** While scale-free patterns can develop in one space dimension, the dynamics in two dimensions clearly show a phase coarsening process (Fig. 7) that results asymptotically in a single circular spot. The major difference between the two cases is the curvature-induced front motion in two dimensions. A

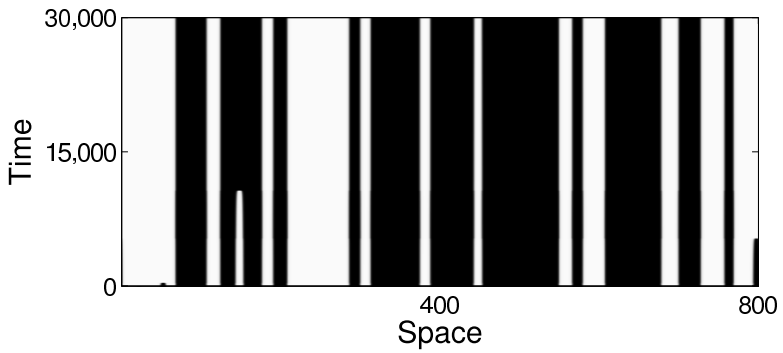

FIGURE 8. A space-time plot, obtained by numerical integration of Eqs. (2) and (9), showing the development of a frozen scale-free pattern in the limit $\delta \to \infty$ of a one-dimensional system. The initial conditions consist of pink noise perturbations about the unstable equilibrium state (u_0, v_0). Parameters: $b = -1$, $c = 0$, $a_0 = -0.15$, $a_1 = 0.5$, $\epsilon = 3.0$

straightforward extension of the one-dimensional analysis to two dimensions, using a coordinate frame that moves with a curved front [29], leads to

$$C_n(s,t) = \alpha v(t) - \kappa(s,t)\,, \tag{19}$$

where C_n is the normal front velocity (velocity component normal to the front line), κ is the front curvature, and s is the arclength coordinate. We defined here the curvature to be positive (negative) for a convex (concave) up-state domain, and assumed that the radius of curvature is much larger than the front width, i.e. $|\kappa| \ll 1$.

Consider now a stationary pattern consisting of an arbitrary number of up-state spot-like domains. Then $C_n = 0$ for any spot and $\kappa = \alpha v$. Note that for an up-state domain $\alpha < 0$ and v should be negative to balance the curvature effect. Since v is independent of space the curvature of any spot should be constant (independent of the arclength), implying a circular geometry. For the same reason all spots should have the same radius. However, a stationary pattern consisting of two or more circular spots of equal size is unstable [23, 24, 25]. The instability of this state can be intuitively understood as follows. Imagine a perturbation that decreases the radius of a given spot. According to (19), the increased curvature will induce a negative normal velocity, causing the spot radius to decrease even further. The local decrease of v opposes this process, but has a negligible effect on relatively small spots because of the immediate homogenization of v which, in turn, causes a slight increase of the radii of other spots. This instability drives the disappearance of small spots and the enlargement of big spots, and accounts for the Ostwald-ripening process shown in Fig. 7. The process culminates in a stable state consisting of a single circular spot. The radius of the asymptotic spot, $R = R_0$, can be found by looking for stationary solutions of Eqs. (9) and (19) written in the form

$$v_t = \epsilon[h(v,R) - a_0 - a_1 v] \tag{20}$$

$$R_t = \alpha v - 1/R\,, \tag{21}$$

where $h(v,R) = \langle u \rangle$. The function h can be approximated as $h \approx [u_+(v)A_+ + u_-(v)A_-]/A$ where A is the total area of the system and $A_\pm$ are the areas occupied by the up state (i.e. the spot area πR^2) and by the down state. The general analytical expression for R_0 is pretty long [30] and we do not present it here, but it agrees very accurately with a calculation based on direct integration of Eqs. (2) and (9). For large systems we find that the spot area $A_+ = \pi R_0^2$ is approximately $A(1+a_0)/2$. We also used Eqs. (21) to study the stability of a single stationary spot solution, and found it to be linearly stable in the parameter range of interest ($\epsilon > \epsilon_H$ and $0 < \kappa \ll 1$).

Ostwald-ripening processes are characterized by power-law growth forms of the average spot radius. Two main growth forms are known: interface-controlled with power law $\bar{R} \sim t^{1/2}$, and diffusion-controlled with power law $\bar{R} \sim t^{1/3}$ [23]. A power law $\bar{R} \sim t^{1/2}$ is known to exist for Eq. (2) with a global constraint, resulting, for example, from mass conservation [23]. We tested this power law with numerical studies of Eqs. (1) and confirmed its validity for these equations too (see also Fig. 4). This implies that vegetation-patch coarsening in the limit of large δ_h is an interface-controlled Ostwald-ripening process.

The phase coarsening shown in Fig. 7 has been found for a supercritical Turing bifurcation, but numerical studies show the occurrence of phase coarsening also in the case of a subcritical bifurcation. Under conditions of finite-range competition, the subcritical Turing bifurcation provides a mechanism, homoclinic snaking [20], that stabilizes isolated spots, as Fig. 6(a) shows. Can this mechanism apply to the case of global competition and thereby prevent the coarsening of scale-free patterns? In an attempt to address this question we considered the limit of fast inhibitor diffusion, $\delta \to \infty$, but increased ϵ too to remain in the snaking range close to the Turing bifurcation (see (5)). This has resulted in the formation of regular patterns with characteristic length, highlighting the importance of the condition $\delta/\epsilon \gg 1$, or fast inhibitor diffusion *relative to inhibitor production*, for the formation of scale free patterns.

4. **Conclusion.**

Observations of vegetation patterns in arid and semi-arid regions have motivated numerous model studies of vegetation pattern formation [9]. Including in the models mechanisms of long range competition over the limited water resource yields finite-wavenumber instabilities of uniform vegetation and vegetation patterns with characteristic length scales, such as hexagonal spot and hole patterns, and stripes patterns [8, 18]. When the competition range is increased to length scales of the order of the system's size, i.e. becomes global, scale-free patterns emerge [6]. On long time scales, however, a slow process of patch coarsening is numerically observed in which small patches shrink and disappear while large patches grow and merge (Fig. 3). The process approaches a single stationary circular patch.

To gain a better understanding of vegetation patch coarsening we first observed that Eqs. (1) represent an activator-inhibitor system, in which the activator corresponds to the above-ground biomass and the inhibitor corresponds to the lack of soil-water. We further observed that this system is qualitatively similar to a simpler activator-inhibitor system described by a modified FitzHugh-Nagumo (FHN) model. In both systems pattern formation results from sufficiently fast transport of the inhibitor. In the FHN model it is the diffusion of the inhibitor from the activator growth area, where it is produced, to the neighborhood of this area, where it inhibits the activator growth. In the vegetation model it is the flow of surface water

towards a growing vegetation patch which inhibits vegetation growth in the patch neighborhood (by inducing lack of soil-water). We then found that the (modified) FHN model reproduces the basic phenomenology of the vegetation model. This includes the sequence of basic states along the control-parameter axis (compare Fig. 1 with Fig. 5), bistability ranges of any consecutive pair of basic states and spatially mixed patterns in these ranges (compare Fig. 2 with Fig. 6), and scale-free patterns that go through phase coarsening in the limit of global competition obtained by fast inhibitor diffusion relative to inhibitor production (compare Fig. 3 with Fig. 7).

Motivated by this close phenomenological analogy between the two models, we used the simpler FHN model to study the phase coarsening process. We found that the limit of global competition corresponds to a Ginzburg-Landau two-phase system subjected to a global constraint. In one space dimension it yields scale free patterns, whereas in two dimensions it shows an interface-controlled Ostwald-ripening process in which the average patch size increases in time like $t^{1/2}$ and the dynamics culminates in a single stationary circular domain. These results suggest that the patch coarsening process observed in the vegetation model is also an example of an interface-controlled Ostwald-ripening process. Indeed numerical computations of the average patch size during this process support a $t^{1/2}$ power law for the average patch radius (or a linear growth of the patch area) as Fig. 4 indicates.

The coarsening of vegetation patches under conditions of global competition may not have significant ecological implications because of the long time scales involved, e.g. thousands of years in the late coarsening stage for a woody species in a system whose size is about 1 km^2. On such long time scales ecosystems are subjected to strong disturbances of various kinds and the states of the undisturbed systems may not be relevant any more. But the observation of Ostwald ripening processes, even in complex models such as the vegetation model, raises an interesting mathematical question: can stationary scale-free patterns in deterministic continuum models exist asymptotically? For that to happen a mechanism that stabilizes small spots should exist. Small spots exist as stable localized structures in the snaking range near a subcritical Turing bifurcation [20, 21] (see Figs. 5(a) and 6(a)). This mechanism, however, is ruled out by the numerical observation that approaching the fast inhibitor-diffusion limit, $\delta \to \infty$, while keeping the system close to the subcritical Turing bifurcation (by increasing ϵ) does not lead to scale free patterns.

Acknowledgments. This research has been supported by the James S. McDonnell Foundation.

REFERENCES

[1] R. A. Brown, *Longitudinal instabilities and secondary flows in the planetary boundary layer: A review*, Rev. of Geophysics and Space Physics, **18** (1980), 683–697.

[2] C. Valentin, J. M. d'Herbès and J. Poesen, *Soil and water components of banded vegetation patterns*, Catena, **37** (1999), 1–24.

[3] T. M. Scanlon, K. C. Kelly, S. A. Levin and I. Rodriguez-Iturbe, *Positive feedbacks promote power-law clustering of Kalahari vegetation*, Nature, **449** (2007), 209–212.

[4] S. Kéfi, M. Rietkerk, C. L. Alados, Y. Pueyo, V. P. Papanastasis, A. ElAich and P. C. de Ruiter, *Spatial vegetation patterns and imminent desertification in Mediterranean arid ecosystems*, Nature, **449** (2007), 213–216.

[5] A. Manor and N. Shnerb, *Facilitation, competition, and vegetation patchiness: From scale free distributions to patterns*, J. Theoretical Biology, **253** (2008), 838–842.

[6] J. von Hardenberg, A. Y. Kletter, H. Yizhaq, J. Nathan and E. Meron, *Periodic versus scale-free patterns in dryland vegetation,* Proc. R. Soc. Lond. B, **277** (2010), 1771–1776.

[7] E. Gilad, J. von Hardenberg, A. Provenzale, M. Shachak and E. Meron, *Ecosystem engineers: from pattern formation to habitat creation*, Phys. Rev. Lett., **93** (2004), 0981051.
[8] E. Gilad, J. von Hardenberg, A. Provenzale, M. Shachak and E. Meron, *A mathematical model for plants as ecosystem engineers*, J. Theor. Biol., **244** (2007), 680–691.
[9] See the following review and references therein: F. Borgogno, P. D'Odorico, F. Laio and L. Ridolfi, *Mathematical models of vegetation pattern formation in ecohydrology*, Reviews of Geophysics, **47** (2009), RG1005.
[10] R. Lefever and O. Lejeune, *On the Origin of tiger bush*, B. Math. Biol., **59** (1997), 263–294.
[11] O. Lejeune, M. Tlidi and R. Lefever, *Vegetation spots and stripes: dissipative structures in arid landscapes*, International Journal of Quantum Chemistry, **98** (2004), 261–271.
[12] M. Rietkerk, M. C. Boerlijst, F. Van Langevelde, R. HilleRisLambers, J. Van de Koppel, L. Kumar, H. H. T. Prins and A. M. De Roos, *Self-organization of vegetation in arid ecosystems*, American Naturalist, **160** (2002), 524–530.
[13] H. Yizhaq, E. Gilad and E. Meron, *Banded vegetation: biological productivity and resilience*, Physica A, **356** (2005), 139–144.
[14] E. Gilad, M. Shachak and E. Meron, *Dynamics and spatial organization of plant communities in water limited systems*, Theoretical Population Biology, **72** (2007), 214–230.
[15] E. Sheffer, H. Yizhaq, E. Gilad, M. Shachak and E. Meron, *Why do plants in resource deprived environments form rings?* Ecological Complexity, **4** (2007), 192–200.
[16] E. Meron, H. Yizhaq and E. Gilad, *Localized structures in dryland vegetation: forms and functions*, Chaos, **17** (2007), 037109.
[17] A. Y. Kletter, J. von Hardenberg, E. Meron and A. Provenzale, *Patterned vegetation and rainfall intermittency*, J. Theoretical Biology, **256** (2009), 574–583.
[18] E. Meron, *Modeling dryland landscapes*, Math. Model. Nat. Phenom., **6** (2011), 163–187.
[19] J. von Hardenberg, E. Meron, M. Shachak and Y. Zarmi, *Diversity of vegetation patterns and desertification*, Phys. Rev. Lett., **87** (2001), 198101.
[20] E. Knobloch, *Spatially localized structures in dissipative systems: open problems*, Nonlinearity, **21** (2008), T45–T60.
[21] D. Lloyd and B. Sandstede, *Localized radial solutions of the Swift-Hohenberg equation*, Nonlinearity, **22** (2009), 485–524.
[22] P. W. Voorhees, *Ostwald ripening of two-phase mixtures*, Annu. Rev. Mat. Sci., **22** (1992), 197–215.
[23] B. Meerson and P. V. Sasorov, *Domain stability, competition, growth, and selection in globally constrained bistable systems*, Phys. Rev. E, **53** (1996), 3491–3494.
[24] L. Schimansky-Geier, Ch. Zülicke1 and E. Schöll, *Domain formation due to Ostwald ripening in bistable systems far from equilibrium*, Z. Phys. B, **84** (1991) 433–441.
[25] J. Rubinstein and P. Sternberg, *Nonlocal reaction-diffusion equations and nucleation*, IMA J. Appl. Math., **48** (1992), 249–264.
[26] M. Conti, B. Meerson, A. Peleg and P. V. Sasorov, *Phase ordering with a global conservation law: Ostwald ripening and coalescence*, Phys. Rev. E, **65** (2002), 046117.
[27] P. Coullet, C. Elphick and D. Repaux, *Nature of spatial chaos*, Phys. Rev. Lett., **58** (1987) 431–434.
[28] C. Elphick, E. Meron and E. A. Spiegel, *Spatiotemporal complexity in traveling wavetrains*, Phys. Rev. Lett., **61** (1988), 496–499.
[29] A. Hagberg and E. Meron, *Order parameter equations for front transitions: Nonuniformly curved fronts*, Physica D, **123** (1998), 460–473.
[30] A. Y. Kletter, "Dynamics of Vegetation Patterns in Water-limited Systems," Ph.D. thesis, Ben-Gurion University, 2010.

Received February 2010; revised September 2010.

E-mail address: kletter@bgu.ac.il
E-mail address: j.vonhardenberg@isac.cnr.it
E-mail address: ehud@bgu.ac.il